ADVANCED MATERIALS
www.advmat.de

# Chiroptical Switching of Electrochromic Polymer Thin Films

*Inho Song,* Liyan You, Ke Chen, Won-June Lee, and Jianguo Mei**

**The interaction between light and chiroptical polymers plays a crucial role in chiroptics, spintronics, and chiral-spin selectivity. Despite considerable successes in creating dissymmetric polymer films, the elucidation of chiroptical activities under electrochemical switching remains unexplored. Here homogeneous chiral electrochromics is reported using chiral assembly of conjugated polymers through a transient solidification process with molecular chiral templates. In their neutral state, the chiral electrochromic polymers directly produce a remarkably dissymmetric polarization-dependent transmittance. The circular dichroism (CD) and dissymmetric transmission can be tuned by adjusting the doping level of the electrochemically active polymer films. Under high levels of oxidation, the chiroptical activities are reversed with strong bleaching in the visible, leading to formation of monosignate CD spectra over the infrared region. The matching between circular polarization handedness and chirality of chiroptical polymers makes a distinct impact on optical contrast and color switching dynamics due to the flipped chiroptical activities through polymer redox reactions. The differential circularly polarized transmission in the chiral see-through display can make a well-resolved color change in human eyes, demonstrating proof-of-concept devices for 3D imaging and information encryption. This work serves as a foundation to develop advanced on-chip fabrication of circular polarization-multiplexed display in flexible and highly integrated platforms.**

## 1. Introduction

Manipulation of a light polarization helicity—the degree of circular polarization—with chiral matter is an attractive route toward realizing the next generation of quantum information technologies.[1–6] To date, there has been rapid progress in the investigation on chiroptical interaction in diverse semiconducting materials; however, typical studies have focused on the helical light–matter interaction related to the charge or spin population of electron itself in the chiral matter. It has yet to be explored to study the dissymmetric optical activities of the semiconducting materials under electrochemical switching in consideration of lattice vibrations and their distortion by the electrons and surrounding ions in redox reactions.

The chiroptical tuning through the electrochemical switching has the potential to innovate polarization-multiplexed displays via their chiral electrochromics. These displays have recently gained attention due to the applications in various fields, including 3D imaging and augmented/virtual reality systems, liquid-crystal display backlighting, high-luminance displays, bioresponsive imaging, optical control, and information encryption.[7–13] Most studies on the circular polarization-modulated displays have predominantly focused on organic light-emitting diodes and liquid-crystal displays.[11–21] Successful helicity modulation of light from chiral electrochromic (EC) materials with the redox reaction have not been demonstrated yet, which is expected to lay a foundation for the circular polarization-multiplexed, energy-saving see-through displays.

Herein, we highlight the first development of an intrinsic, chiral electrochromics from redox-active polymer films by a chiral templating approach, in which a small chiral molecule is used to assist the formation of the dissymmetric active layer. The chiral nature of polymer assemblies was induced by rapid chiral orientation without extra high-energy heat or electric/magnetic field. The blue-colored, chiral EC polymer (ECP-Blue) are highly dissymmetric with high CD signal (≈13 000 mdeg) in the neutral state. The intrinsic chiroptical behavior allowed a significant polarization-dependent transmittance and a natural color change depending on the CP handedness. With electrochemical switching in the chiral polymer films, the obvious bisignate CD spectra attenuated with strong visible bleaching, finally leading to a reversible inversion of the sign of the chiroptical effect. The synchronizing between circular polarization and polymer chirality makes largely differential optical contrast and color switching dynamics. Under ambient light conditions, the chiral EC films allow a noticeable color perturbation in the human eye, functioning as a chiral transmissive display. This paves the way for the highly promising application of these newly developed homochiral EC systems in 3D imaging and information encryption.

I. Song, L. You, K. Chen, W.-J. Lee, J. Mei
Department of Chemistry
Purdue University
West Lafayette, IN 47907, USA
E-mail: song735@purdue.edu; jgmei@purdue.edu

The ORCID identification number(s) for the author(s) of this article can be found under https://doi.org/10.1002/adma.202307057



**DOI: 10.1002/adma.202307057**

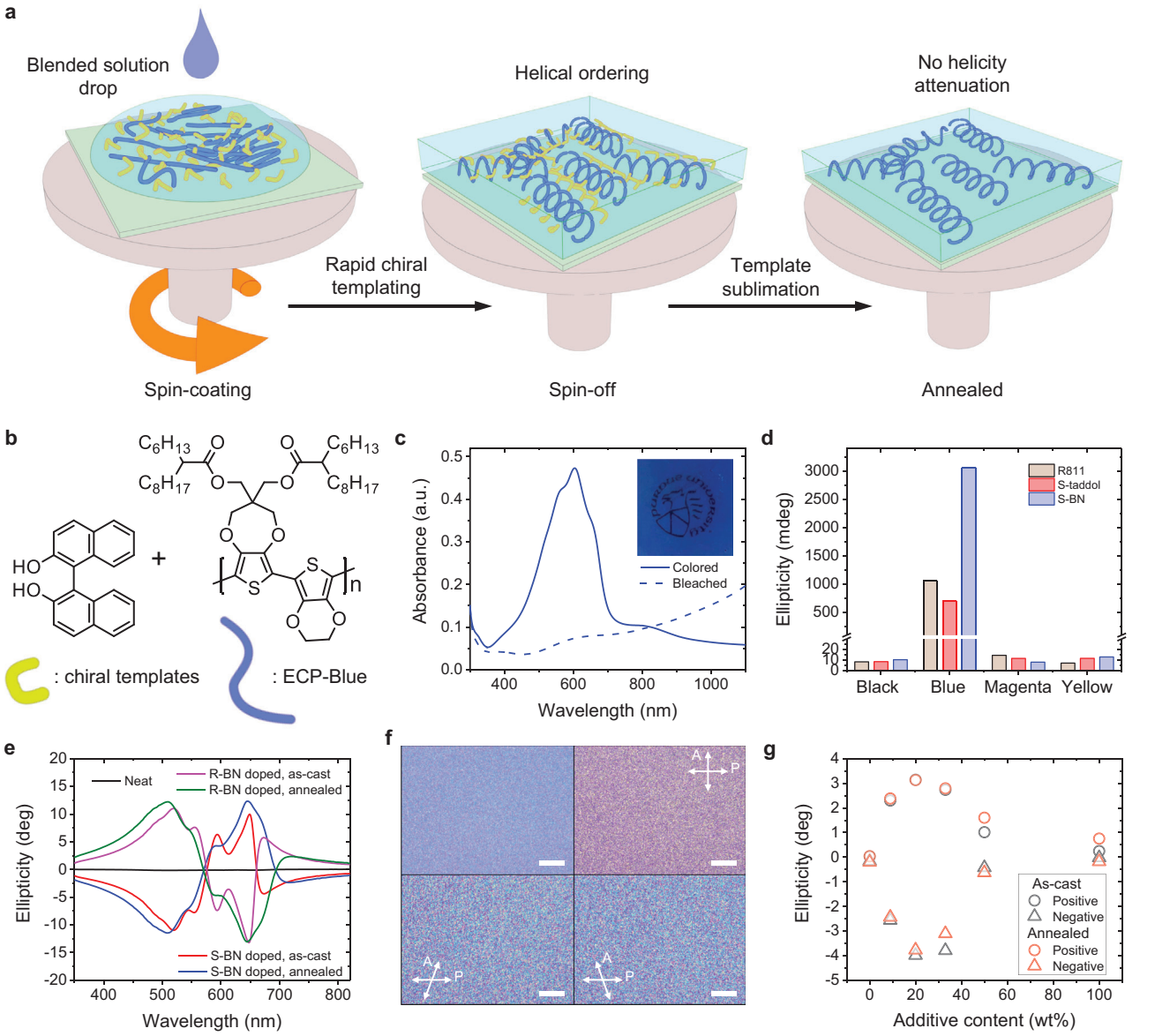


**Figure 1.** Chiroptical properties of chiral EC polymer films. a) Schematic of chiral transient templating using molecular chiral templates and long-range ordered conjugated polymers. No heat or electric/magnetic field are needed to induce the chiral ordering of achiral polymers. Template sublimation by annealing treatment does not attenuate the chiroptical properties. b) Molecular structures of the blue EC polymer and the chiral BN additive. c) Optical absorbance spectra of ECP-Blue films in the reduced and oxidized states. Inset Figure shows photographic image of ECP-Blue film at the reduced state. d) Maximum ellipticity intensity recorded in diverse chiral templated EC polymer films on quartz plate. e) Optimized ellipticity spectra of the templated ECP-Blue films (25 wt% BN additives, ≈350 nm) before and after thermal annealing. f) Bright optical microscopy and polarizing optical microscopy images (i.e., degree of cross polarizers = 90°, 45°, and 135°) of the templated ECP-Blue films blended with *S*-BN after thermal annealing. Scale bars show 20 µm. g) Maximum ellipticity intensity of the templated ECP-Blue films before and after thermal annealing depending on the ratio of chiral BN additives.

## 2. Results and Discussion

### 2.1. Electrochromic Chiral Polymer Films

To develop the highly dissymmetric, electrochemically active polymer thin films, we introduced the chiral templating method by blending chiral additives (dopants) into achiral EC polymers (**Figure 1**a). Four conjugated polymers based on poly(3,4-propylenedioxythiophene) (PProDOT), which are commonly used in EC applications were initially tested for the formation of chiral structures through the templating method. In the absence of chiral additives, the four colors of EC polymers (ECP-Black, ECP-Blue, ECP-Magenta, and ECP-Yellow) showed reversible absorbance changes during the redox process. With a positive bias applied, they exhibited a significant decrease in visible-absorbance, along with a color change from black, blue, magenta, and yellow to transmissive, respectively (Figure 1b,c; Figure S1, Supporting Information).

To test whether chiral templating can lead to dissymmetric polymer thin films, three chiral additives, whose molecular structures and names are depicted in Figures S1 and S2 (Supporting Information), were blended with four polymers above. Briefly, chiral additives and polymers at a specific ratio were dissolved in chloroform. All solutions were then spin-coated on quartz plates and the obtained thin films (≈200 nm) were subjected to CD measurements. Among all combinations, only ECP-Blue presented intense CD signals (Figure 1d; Figure S3, Supporting Information), while others either showed no chiral response or exhibited a weak Cotton effect in absorption region of the conjugated polymers (i.e., ECP-Magenta with (−)−4,5-Bis[hydroxy(diphenyl)methyl]−2,2-dimethyl-1,3-dioxolane [*S*-taddol] and (R)-Octan-2-yl 4-((4-(hexyloxy)benzoyl)oxy)benzoate [R811]; ECP-Yellow with *S*-taddol and (S)−(−)−1,1'-Bi(2-naphthol) [*S*-BN]) with their CD intensities less than 20 mdeg. It is worth noting that the chiral BN templated ECP-Blue thin films generated the strongest signate CD signal (≈13 000 mdeg; ≈0.21 of $g_{abs}$) in the visible absorption band of ECP-Blue with optimized thicker films (thickness ≈ 350 nm; Figure 1e; Figure S4, Supporting Information). This value is among the highest in chiral polymers. The CD-effective region did not originate from the chiral additive itself (Figure S5, Supporting Information), which is indicative of the chirality transfer and amplification from the chiral additives to whole blended systems. This is supported by the polarized optical study, in which pronounced birefringent textures were observed in the ECP-Blue films. The birefringence indicates the presence of long-range molecular ordering (Figure 1f; Figure S6).[22–24] Chiral conformation in the long-range ordered polymer films was dominantly induced by interactions with the chiral additives, resulting in the amplified chiroptical properties depending on the chiral composition of the templates. The other EC polymer films did not show any anisotropic or birefringent domains (Figure S7, Supporting Information). In addition, atomic force microscopy (AFM) was used to observe surface morphological changes during the chiral templating at microscale (Figure S8, Supporting Information). All polymer films exhibited similar morphologies with small nanobeads, suggesting that chiral templating and thermal annealing did not significantly impact the microscale morphologies in ECP-Blue films. In order to investigate molecular packing within the polymer films, we utilized X-ray diffraction techniques. Figures S9 and S10 (Supporting Information) present the results of grazing-incidence X-ray diffraction (GIXD) analysis. Chiral templating led to the emergence of distinctive crystalline diffraction in as-casted samples. However, the new diffraction pattern vanished upon thermal annealing, indicating that this diffraction pattern was associated with chiral dopant itself. Excluding the diffraction peaks from the chiral small molecule crystals, the polymer films exhibited weakly diffracting lamellar peaks along the out-of-plane ($q_z$) direction and in-plane $\pi$–$\pi$ packing peaks (Table S1, Supporting Information).[25] Interestingly, the introduction of chiral additives induced denser packing in both lamellar and $\pi$–$\pi$ packing stacking, indicative of the formation of relatively distorted, herringbone motif due to intermolecular interactions with the dopants.[26] Despite the sublimation of the chiral templating molecules, the $\pi$–$\pi$ stacking distances further decreased, suggesting that the chiral films retained their molecular ordering formed with the chiral additives.

To investigate the interactions between the ECP-Blue and different chiral templates, the chiral templating was confirmed in the Fourier transform infrared (FTIR) spectra of the templated ECP-Blue films. The peak at 1730 $cm^{-1}$ corresponding to the C═O stretching from ECP-Blue showed distinct changes by the intermolecular interactions with the different chiral additives (Figure S11, Supporting Information). The templating using R811, *R*-taddol, and *S*-taddol showed neglectable changes in the C═O stretching, although R811 induced additional, blue-shifted C═O stretch from R811 itself. On the other hand, both R-BN and S-BN templating caused broadening and reduction in the C═O stretching peak, suggesting some of the polymer chains strongly interact with the BN molecules via hydrogen bonding between the ketone and the hydroxyl group.[27,28] Additionally, four chiral BN derivatives (as shown in Figure S2c–f in the Supporting Information) were evaluated for the chiral templating. Upon the optimization, the parent BN exhibited the highest CD amplification due to their strong intermolecular noncovalent interactions with the conjugated polymers (Figure S12, Supporting Information).

Interestingly, our chiral templating is rapidly realized in the transient solidification during the removal of the low-boiling point solvent in the spin-coating process, contrasting with previous methods that relied on either high thermal energy or slow chiral chain rearrangement.[21,29,30] Chiral BN sublimation in the range of 160–240 °C did not attenuate the chiroptical activities of polymer films as observed in CD spectra, but accordingly the optical absorbance at UV region from the template molecule is absent with its removal (Figure S13, Supporting Information). On the other hand, the thermal annealing resulted in slight broadenings and red-shifts of absorption and CD peaks due to a stronger intermolecular aggregation in polymer chains (Figure S14, Supporting Information). It was found that 20–35 wt% of chiral additives in the blends provided the strongest chiroptical response, as shown in Figure 1g and Figure S15 (Supporting Information), while the excess additive loading could disrupt the chiral conformation of polymer chains, leading to a significant decrease in ellipticity.

### 2.2. Chiroptical Properties Under Electrochemical Switching

The EC devices were assembled with a standard configuration ITO/counter electrode (CE)/electrolyte/ECP/ITO, in which $VO_x$ served as the charge-balancing material (CE), electrolyte was made from polyethylene glycol diacrylate (PEGDA):lithium bis(trifluoromethanesulfonyl)imide (LiTFSI), and the ECP layer was chiral ECP-Blue templated by chiral BN additive. Further details on the device fabrication and characterization of the chiral EC films are given in the Experimental Section. In the cyclic voltammetry measurements, the pristine (achiral) and chiral films showed almost identical curve shapes, peak positions, and oxidation onsets, which indicates that they possess a similar electrochemical reaction (Figure S16, Supporting Information). **Figure 2**a,b and Figure S17a (Supporting Information) show the optical absorption of the chiral EC films with left- and

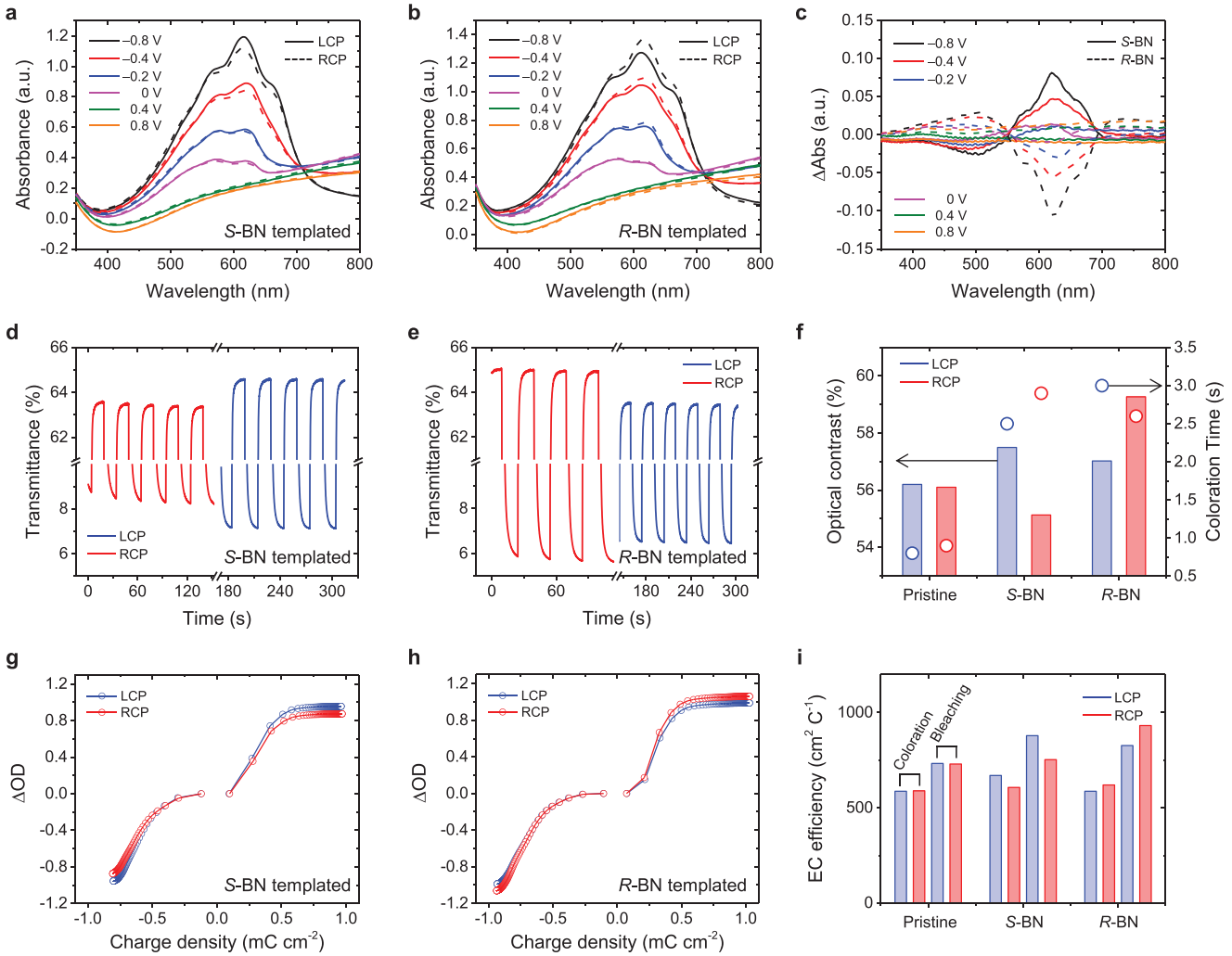


**Figure 2.** Dissymmetric chiroptical behavior of chiral templated ECP-Blue EC devices. a,b) Optical absorbance of *S*-BN (a) and *R*-BN (b) templated ECP-Blue EC devices after thermal annealing upon the left- (solid line) and right-handed (dotted line) circularly polarized light. c) Differential optical absorbance of *S*-BN (solid line) and *R*-BN (dotted line) templated ECP-Blue EC devices after thermal annealing. d,e) Optical transmittance of *S*-BN (d) and *R*-BN (e) templated ECP-Blue EC devices upon the left- (blue) and right-handed (red) circularly polarized light after thermal annealing. f) Optical contrast and dynamic coloration rate of chiral templated ECP-Blue EC devices upon the left- (blue) and right-handed (red) circularly polarized light. g,h) Optical contrast change as a function of charge density in bleaching and coloration process of annealed *S*-BN (g) and *R*-BN (h) templated ECP-Blue films. i) Bleaching and coloration efficiency of annealed chiral templated ECP-Blue films.

right-handed circularly polarized beams. Interestingly, *S*-BN templated EC devices showed a larger absorption under the left-handed circularly polarized beam in the neutral state, while *R*-BN EC devices gave a larger absorption under the right-handed beam. As compared to achiral ECP-Blue films (Figure S18, Supporting Information), the CD (i.e., differential absorption) signals of the chiral templated films were prominent. As summarized in Figure 2c, the chiral templated ECP-Blue films exhibited mirror-imaged differential absorption depending on the chiral composition of the molecular templates. The *S*-BN templated ECP-Blue films showed a positive CD at a longer wavelength (645 nm) and a negative one at a shorter wavelength (510 nm), which is indicative of a clockwise screw sense in the chromophore constitution. The *R*-BN templated films showed mirror-imaged spectra, leading to counterclockwise stacking for transition dipoles.

With applying the potential from −0.8 to 0 V, the EC devices were gradually bleached as the EC polymer is being doped. Accordingly, the bisignate, mirror-imaged CD spectra could be attenuated (Figure 2c; Figure S19, Supporting Information). Thus, it indicates that the CD signal originated from the intrinsic exciton chirality in chiral polymer films,[31] rather than from the artificial CD.[32] In the chiral exciton coupling, the intensity of the exciton CD is proportional to the square of the absorption coefficient, $\epsilon$, of the polymer.[33] The absorption coefficient of the polymer decreases as the ECP-Blue oxidizes,[34] leading to the decrease in the bisignate CD intensity in our chiral films. In the intrinsically generated chiroptical activities, the CD-active region is synchronized with the polymer absorption profile, enabling a

natural CD modulation through electrochemical switching of chiral ECP-Blue films. The chiral templated films without thermal treatment showed similar chiroptical electrochemical behaviors compared to those of annealed films (Figure S20, Supporting Information). We confirmed that the electroactive CD after redox reactions has slightly different peak positions as compared to that before the redox reactions (Figure S21a–c, Supporting Information). The formation of favorable pathways for ionic movement during the electrochemical activities leads to small morphological and consequent chiroptical changes (i.e., "break-in").[35] The $g_{trans}$ values estimated from UV–vis–NIR spectrophotometer customed with circular polarization lenses showed similar trends with those from conventional CD spectrometer (Figure S21d, Supporting Information).

As the applied voltage continues to increase to 0.4 and 0.8 V, ECP-Blue became fully doped, leading to a significant reduction in their CD intensities. At high doping levels, only broad, monosignate CD spectra were observed in the short-wave infrared (SWIR) region (Figure S22, Supporting Information). The presence of monosignate CD spectra suggests potential chiroptical activities in the polaron band. The polarons exhibited strong localization along the polymer chains due to the strong electrostatic coulomb binding to anions[36] as well as a robust electron–phonon coupling.[37] While highly delocalized excitons in chiral stacks can generate strong degenerate coupling, leading to the splitting of excitonic states into a high-energy (*H*-aggregate) and low-energy state (*J*-aggregate) with subsequent bisignate CD features,[31] this phenomenon was not observed in the strongly localized polarons at the charged quinonoid structures.[38] Consequently, the CD signal in this polaron band arises from the nondegenerate transition dipoles, resulting in observed monosignate CD spectra at the highly electrochemically-doped state.[39]

Figure 2d,e and Figure S17b (Supporting Information) compare double potential step chronoabsorptometry (DPSC) of pristine and chiral templated films (+1 V to −0.8 V, $\lambda$ = 615 nm). *S*-BN templated EC devices showed low transmittance under the left-handed circularly polarized light at the reduced state, but inversely have high transmittance under the left-handed one at highly oxidized state. On the other hand, *R*-BN templated devices displayed opposite behavior, with high transmittance in the reduced state and low transmittance in the oxidized state under left-handed beam. In other words, the chiral templated ECP-Blue films clearly exhibited the inversion of the sign of chiroptical activities in the visible region between oxidized and reduced states, leading to a larger transmittance contrast ($\Delta\%T$) of around 3% depending on the circular polarization handedness of the incident beam. The coloration and bleaching switching rates in the electrochemical doping were evaluated as function of time to reach 95% of the full transmittance contrast, $t_{95\%}$ (Figure S23, Supporting Information). The coloration rates of the chiral templated films were also changed by the incidence of different handedness of the circularly polarized beam (Figure 2f). Interestingly, it was confirmed that the optical switching becomes faster as well as the EC optical contrast increases. The *S*-BN templated ECP-Blue films exhibited faster transmittance changes in coloration process under the left-handed CP light transmission, which may be related to larger differential beam absorption changes at the same redox reaction rate.

The pristine (achiral) ECP-Blue devices showed the negligible changes in $\Delta\%T$ and $t_{95\%}$ under different circular polarization. Compared to the pristine film, however, the chiral templating decreased the switching speed, especially in the coloration process. The chiral templating mainly affects the EC dynamics in the coloration stage, where electrolyte ions migrate out of the polymer film to maintain charge neutrality in the dedoping process. The morphological changes caused by the chiral templating perturb the ionic movement pathways for anion dissociation in the reduction process. However, chiral ECP-Blue films demonstrated remarkable electrical and optical stability despite the introduction of chiral dopants. All ECP-Blue films exhibited minimal changes in transmittance ($\Delta T < 0.7\%$) during 1-h EC cycling (Figure S24, Supporting Information). To study the switching response of the electrochemical reaction, chronoamperometry (CA) curves of ECP films were recorded at the same potential step condition as the DPSC characterization (Figure S25, Supporting Information). The achiral ECP-Blue films showed a higher transient current density than the chiral templated ones for electrochemical redox reactions. Accordingly, the slightly better coloration efficiency (≈600 $cm^2$ $C^{-1}$ for coloration and ≈900 $cm^2$ $C^{-1}$ for bleaching) could be observed in the chiral templated films due to their small charge intercalation and extraction (Figure 2g–i; Figure S26, Supporting Information). It should be noted that chiral templated ECP films exhibited differential coloration and bleaching efficiencies with respect to the polarization handedness of the transmitted beam. It resulted from the larger and faster optical contrast changes upon the polarization handedness during the polarization-independent electrical charge accumulation. In short, the color switching dynamics, optical contrast, and electrochemical charge extraction of EC devices could be modulated depending on the circular polarization handedness and chirality of templating molecules.

### 2.3. Dissymmetric Circularly Polarized Transmission

To demonstrate the feasibility of circularly polarized transmission through chiral EC films, we employed nonchiral light irradiation to record their differential transmission. We utilized a circular polarization filter, consisting of a linear polarizer and quarter-waveplate, positioned between the chiral polymer films and the photodetector of the absorption spectrometer to quantify the circular polarization content (**Figure 3**a). Remarkably, the chiral templated ECP-Blue films exhibited mirror-imaged differential transmittance in the undoped state (Figure 3b,c; Figure S27, Supporting Information). This indicates that these films serve as excellent chiral transmissive filters, capable of generating well-resolved circularly polarized light transmission from unpolarized ambient light. Furthermore, upon oxidation of chiral electrochemical polymers, we observed a significant sign inversion in the visible region of the differential transmittance spectra. This inversion was particularly evident in the dynamic transmittance difference with respect to circular polarization ($\Delta\%T \approx$ 7%), as characterized by DPSC (Figure 3d). The extremely large chiroptical activities of ≈13 000 mdeg resulted in intrinsic optical perturbation that could even be detected by the human eye, depending on circular polarization handedness. Tristimulus values, which represent the sensitivity of the cone cells in the human

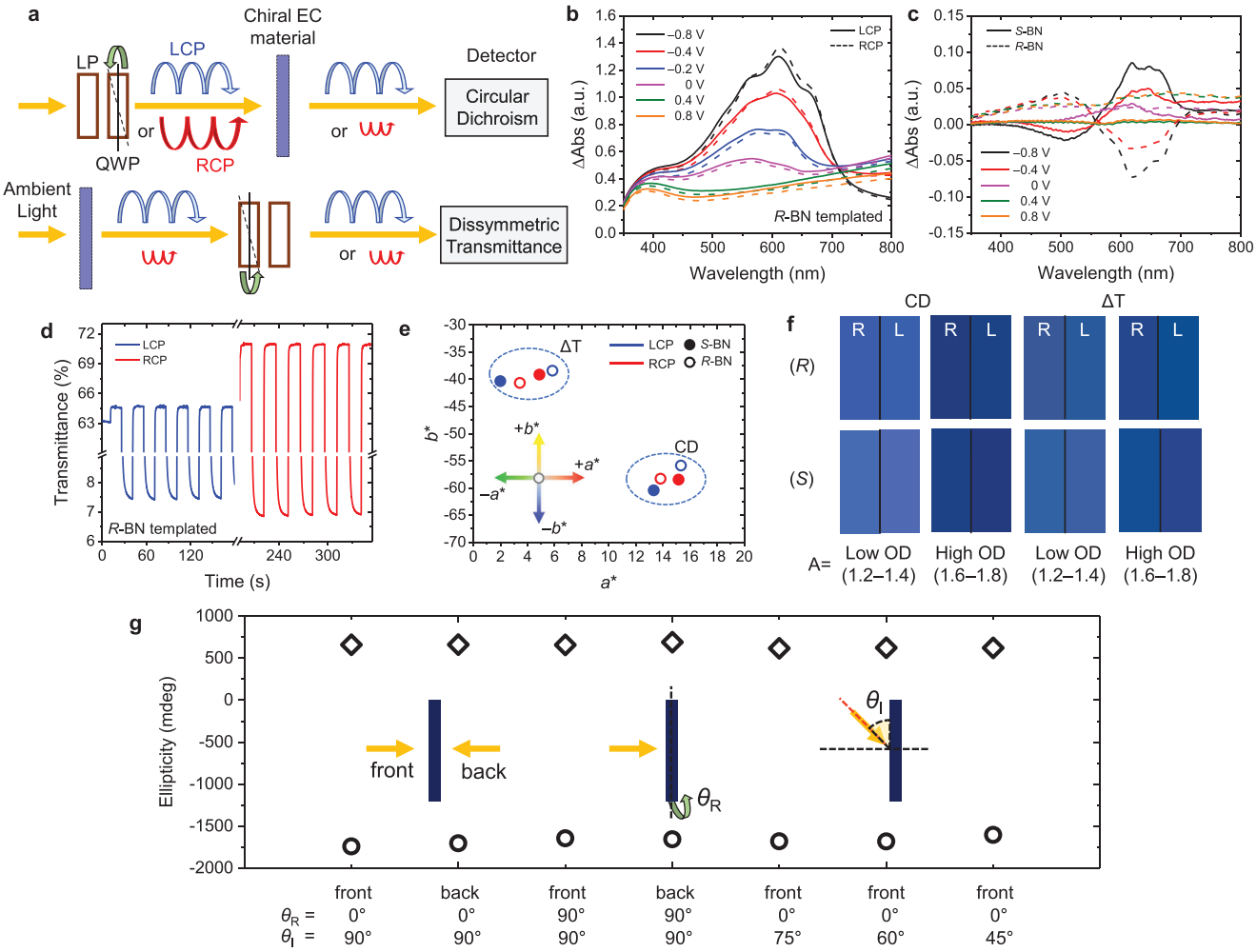


**Figure 3.** Dissymmetric circularly polarized transmittance in see-through chiral EC display devices. a) Two different measurement methods for CD (top) and dissymmetric transmittance (bottom) of chiral EC films. b) Optical absorbance of *R*-BN templated ECP-Blue EC devices after thermal annealing recorded through the left- (solid line) and right-handed (dotted line) circularly polarized light filter. c) Dissymmetric light transmission of *S*-BN (solid line) and *R*-BN (dotted line) templated ECP-blue EC devices after thermal annealing. d) Dynamic optical transmittance changes of *R*-BN templated ECP-Blue EC devices after thermal annealing through the left- (blue) and right-handed (red) circularly polarized light filter. e) CIE $a^*$ and $b^*$ color coordinate values of chiral templated ECP-Blue EC devices. Inset shows color hues of $a^*$ and $b^*$ color indicators. f) Reconstructed colors from $L^*a^*b^*$ system from absorbance spectra of chiral templated ECP-Blue EC devices recorded. g) Maximum ellipticity of *R*-BN templated ECP-Blue films considering the azimuthal rotation/flipping of samples and the angle of incident light. Diamond means positive maximum, and circle means negative one in bisignate CD spectra.

eye, were estimated using the CD and the dissymmetric transmittance measurement (1976 CIE $L^*a^*b^*$; Figure 3e). In the color space, $L^*$ corresponds to the perception of lightness, while the $a^*$ and $b^*$ axes define the chromaticity, each ranging from 0 to 100.[40] In a 2D chromaticity space (inset of Figure 3e), $+a^*$ and $-a^*$ values indicate color with red and green hues, respectively. Meanwhile, the $b^*$ axis represent yellow at positive point and blue at negative point. The calculated chromaticity values of the chiral templated films varied with different circular polarization handedness in both measurement setups. Importantly, the dissymmetric optical properties were expressed as changes in chromaticity rather than brightness in the 3D color space (Figure S28, Supporting Information). Specifically, the right-handed circularly polarized light resulted in a reduction of $b^*$ value and an increase in $a^*$ value for *S*-BN templated EC films, while the left-handed beam resulted in the similar color changes for *R*-BN templated ones. This indicates that the pure blue hues (related to $-b^*$) of the ECP-Blue films were attenuated when circular polarization handedness and chirality of transmissive matter were not matched. The color estimated from $L^*a^*b^*$ values demonstrated recognizable color changes visible to the human eye in chiral polymer films with different optical densities, highlighting their potential for chiral transmissive displays utilizing optical perturbation under ambient light irradiance (Figure 3f).

To ensure a wide viewing angle and maintaining a constant polarization in transmissive displays that utilize random outdoor light as a light source, it is crucial to demonstrate an isotropic chiroptical property irrespective of the incident light–matter interaction conditions such as azimuthal sample rotation, sample flipping, and varied beam incidence angle. The interaction

between ambient light and the anisotropic nature of the material can give rise to artificial CD (Equation and detailed explanation are summarized in the Experimental Section).[31] In outdoor applications, the detrimental impact of anisotropic CD on differential transmittance can be amplified due to the interaction with versatile circular and linear polarization of random ambient light. To address this, we first investigated the influence of sample flipping. We found that there were negligible differences in the positive and negative maxima across the entire CD spectral range when the sample was flipped (i.e., front vs back in Figure 3g and Figure S29, Supporting Information). This observation indicates that the artificial CD based on the macroscopic anisotropic effect in the chiral active layer was minimal.[22] Furthermore, we investigated the effect of rotating the azimuthal angle of the mounted sample around the optical axis of the incident light (denoted as $\theta_R$). We observed no change in the CD signal, which suggests that the residual linear polarization did not contribute to the artificial CD. Overall, these findings highlight the high feasibility of utilizing circularly polarized transmission for real see-through chiral display applications. By minimizing the contributions of artificial CD, such displays can offer enhanced performance and functionality. In certain chiral media based on a periodic helicoidal structure, the optical responses remain unchanged when the sample or the beam polarization axis is rotated along the azimuth.[41] However, there are notable differences in the optical behavior depending on the incident angle of the beam. These chiral media exhibit a decrease in CD intensity as the incident angle decreases. Additionally, there is a significant shift in the spectral optical response described by the equation, $\lambda = \lambda_0 \cos\theta$, where $\theta$ represents the angle of incidence and $\lambda_0$ corresponds to the peak position at normal incidence.[42] In electronic CD measurement, our chiral EC films displayed consistent chiroptical properties when the angle of incident light (i.e., $\theta_I$) varied from 90° to 45° within the plane parallel to the sample orientation. This characteristic is crucial for expanding the viewing angle in chiral EC display application.

### 2.4. Chiroptical Electrochromic Display

Finally, a circular polarization-encoded EC display was created by selectively patterning chiral templated ECP-Blue films using standard photolithography techniques (See the Experimental Section for detail). Chiral ECP films were selectively patterned to display millimeter-sized grid-pattern images (square pattern of 1.0 mm). To read the encoded circularly polarized transmission, a quarter waveplate and linear polarizer were placed between the chiral templated EC display and a digital camera. These components acted as a circular polarization filter, selectively blocking one-handedness circularly polarized light depending on the cross angle between the lenses. By rotating the cross angle, an observable image change was achieved after passing through the circular polarization filter. This concept holds potential for polarization-encoded 3D display with circular polarization filtered glasses (**Figure 4**a). In Figure 4b, the images measured at −45° (left) and +45° (right) cross angles demonstrated distinct differential colors in the grid-patterned chiral films, depending on matching between the polarization handedness of the filters and the chiral composition of the films. Consequently, the two images from a single segment display could be separated to enter the left and right human eyes after passing through opposite circular polarization lenses, resulting in binocular disparity and an immersive 3D sensation for viewers.[11]

A more sophisticated segment-type EC display with a "train" image was prepared by patterning chiral ECP-Blue films, which could be colored and bleached by the external electric bias (−1.0 V for colored and +1.0 V for bleached state) as shown in Figure S30 in the Supporting Information. Figure 4c displays photographic results after circular polarization filtering, revealing differential colors with low crosstalk observed at the positions of the left and right human eyes, even in microsized patterns. Furthermore, the circular polarization-encoded images could be hidden from native eye as demonstrated through using linear polarization filtering (i.e., zero cross angle between waveplate and linear polarizer), which showcased a successful proof-of-concept for information encryption and anti-counterfeit concepts using circular polarization encoding. The circular polarization-modulated transmission and information encryption in chiral EC displays were further verified by rotating the waveplate angle of the circular polarization filter in front of the digital camera (Movie S1, Supporting Information).

The operation of the chiral transmissive display was tested under various ambient conditions, including artificial daylight (D65), store light (TL84), and home light (Type A incandescent), as shown in Figure 4b,c and Figure S31 in the Supporting Information. The chiral EC films exhibited excellent circularly polarized transmission and encryption ability in all light irradiations, highlighting their potential for use in diverse real-life ambient light conditions. Furthermore, the chiral EC films demonstrated consistent differential circularly polarized transmission regardless of the rotation of the polarization axis and the viewing angle of the observer (Figures S32 and S33, Supporting Information). This characteristic allows spectators to observe the circularly polarized transmissive image without experiencing crosstalk or a double image caused by a mismatch of the polarization axis between the display and the circular polarization filter, as well as incorrect positioning of the observer. Thanks to the distinct circularly polarized transmission without crosstalk and the easy integration and patterning capabilities of chiral EC polymers, the projection of the polarization-selective EC images enabled the 3D imaging and information encryption in chiral transmissive display applications.

## 3. Conclusion

In this work, we present highly dissymmetric chiroptical activities in electrochemically active polymers that exhibit inherent circularly polarized transmission. These chiroptical activities arise from the chiral ordering of polymer chains during the rapid solidification process in the presence of molecular chiral templates. The chiroptical properties of the polymers can be controlled through electrochemical switching. We uncovered the significant flipping of the chiroptical activities when the polymers were highly doped, resulting in a transition from featured bisignate CD spectra to monosignate CD spectra. One important observation is the synchronization between the circular polarization handedness and the chirality of the chiral polymers, which leads to substantial changes in optical contrast and color switching

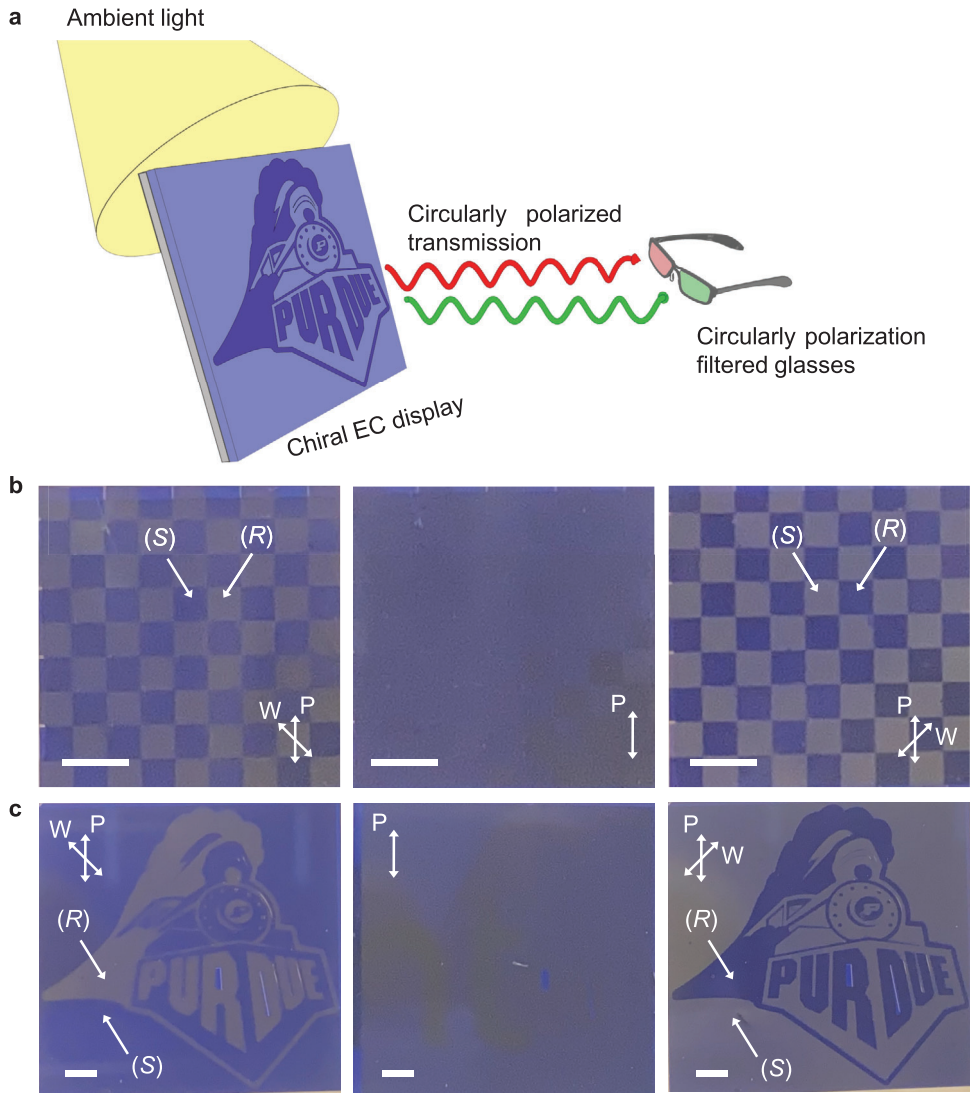


**Figure 4.** Chiral EC display application using circularly polarized transmission. a) Schematic of polarization-sensitive EC image projection in transmissive display for 3D imaging. b,c) Photographic images of chiral EC displays by patterning chiral templated EC polymer with differential handedness into grid-type square pixels (b) and "Train"-shaped segment image (c) for proof-of-concept demonstration in 3D imaging and information encryption. Different circular polarization filters were placed between chiral EC display and a picture capturing digital camera. P indicates a polarization axis of linear polarizer and W indicates a fast axis of quarter waveplate. Type A incandescent, home light was used as light source for ambient condition demonstration. Scale bars indicate 2 mm in all figures.

dynamics. The highly dissymmetric circularly polarized transmission, reaching around 13 000 mdeg, induces noticeable optical perturbations when passing through the circular polarization filters, even to the naked human eye. This was confirmed through the changes in tristimulus values and photographic color. The isotropic chiroptical activities of the electrochemically active polymers are not affected by random polarization or the incidence angle of the irradiated light, thanks to their homogeneous and intrinsic CD behavior. Notably, we report, for the first time, the development of a circular polarization-transmissive display based on the chiral electrochemically active polymers, without the need for additional optical elements. This chiral EC display demonstrates excellent compatibility with wide viewing angle and no crosstalk under varied ambient light irradiation conditions. By leveraging the simplicity and processability of chiral polymers, our pioneering findings open up the way for compact circular polarization-encoded see-through displays that can be implemented on flexible and highly integrated on-chip platforms.

## 4. Experimental Section

*Materials*: LiTFSI salt, propylene carbonate (PC), PEGDA, 2-hydroxy-2-methylpropiophenone (HMPP), and R811 were obtained from Sigma–Aldrich. S-taddol were supplied by Alfa Aesar. Other chiral additives were purchased from Combi-Blocks. EC polymers were provided by Ambilight. All materials were used as received unless otherwise stated.

*Characterization*: All additive-blended polymeric solutions (20–40 mg $mL^{-1}$ in chloroform) were spin-coated on quartz plates at 400–2000 rpm

to obtain the desired film thickness without further treatment for CD and UV–vis–IR spectroscopic measurements except for post-thermal annealing at 200 °C (80–240 °C for annealing temperature-dependent experiments). Polarized optical microscopic images were obtained using an Olympus BX51 microscope equipped with polarizers oriented in a crossed arrangement. Absorption spectra were recorded using a Cary 5000 UV–vis–NIR spectrophotometer (Agilent Technologies). Electrochemical characteristics were recorded using a Biologic SP-150 potentiostat. AFM results were obtained using Cypher Asylum AFM and processed through Gwyddion Software. Polymer films spin coated on silicon substrates were analyzed using GIXD at the Advanced Photon Source at Argonne National Laboratory. Incident beam energy of 10.92 keV was used to collect the diffraction data on a 2D detector, with sample-to-detector distance of 217 mm. FTIR spectra were recorded using Thermo Nicolet 6700 FTIR. Ellipticity spectra were collected using J-1500 circular dichroism spectropolarimeters (JASCO). The $g_{abs}$ values are typically defined using absorption and ellipticity spectra recorded with the J-1500 by the following equation

$$g_{abs} = \frac{\Theta\,(m\,\mathrm{deg})}{32980 \times \mathrm{Abs}} \tag{1}$$

*Fabrication of Chiral Templated Polymer Films*: All polymers (20–40 mg) were dissolved in 1 mL chloroform and stirred continuously overnight. The chiral additives were blended according to the indicated weight ratio. Standard devices were fabricated with 25 wt% of chiral BN blended into polymer solution. Indium-tin oxide (ITO)-coated glass were rinsed using water with 1% detergent, deionized water, acetone, and isopropyl alcohol for 10 min per step. The prepared EC polymer solutions were spin-coated on the ITO substrate, and then annealed at 200 °C for 10 min. The $VO_x$-based ion storage layer was fabricated on the other pre-rinsed ITO substrate according to the reported method.[43] PEGDA, PC with 0.2 M LiTFSI, and HMPP were mixed in a volume ratio of 5:5:1. After stirring for 10 min, the solution was dropped on the ion storage layer deposited ITO substrate. The EC polymer deposited ITO substrate was transferred to the top after flipping. After waiting a few seconds for the electrolyte precursor solution to become uniform, the electrolyte was crosslinked under the UV light irradiation for 15 min. For electrical contact, copper tape was applied to both sides of the ITO.

*Chiroptical Spectra Measurements*: The differential absorbance spectra of chiral EC devices were measured using a Cary 5000 UV–vis–NIR spectrophotometer customized with SP-150 potentiostat and circular polarization filter with linear polarizer and quarter-wave plate (Thorlabs). To measure circular dichroism, the chiral filter was placed between the light source and the sample. To measure dissymmetric transmission, the reversed chiral filter (i.e., light transmitted from the sample passed through the waveplate and linear polarizer, in turn) was placed between the sample and the photodetector of the spectrometer. The $g_{trans}$ values are defined using two absorption spectra recorded with the Cary 5000 UV–vis–NIR spectrophotometer with circular polarization filter by the following equation

$$g_{trans} = \frac{2\,(I_{LCP} - I_{RCP})}{(I_{LCP} + I_{RCP})} \tag{2}$$

$I_{LCP}$ and $I_{RCP}$ denote recorded optical absorbance using UV–vis–NIR spectrophotometer after passing through left-handed and right-handed circular polarization lenses, respectively.

*Patterning of Chiral EC Polymer Films*: The patterning of chiral EC polymer films was demonstrated using conventional photolithography in combination with dry reactive ion etching (RIE) process. AZ1518 (Microchemicals) was spin-coated on the predeposited *S*-BN templated ECP-Blue film as an etch blocking layer (4000 rpm, 45 s) and baked at 110 °C for 2 min to remove residual solvent. The photoresist films were then exposed to the near-UV light (405 nm, 100 mJ $cm^{-2}$) using a maskless aligner (Heidelberg MLA150). The films were developed in developer solution (Microposit, MF-26A) for 45 s. After rinsing with DI water, the patterned films were exposed to etching plasma for 30 min to remove the unprotected polymer layer. The *R*-BN templated EC solutions were spin-coated. Then the photoresist solutions were deposited and patterned in the same way. After plasma etching, all the remaining photoresist films were removed with acetone.

*Interpretation of CD Signal According to Mueller Matrix*: Mueller matrix analysis indicates that the CD signal observed in electronic CD spectroscopy for anisotropic solid samples can be described by the following equation[32]

$$\begin{aligned} \mathrm{CD_{obs}} \approx\ & \mathrm{CD_{iso}} + \frac{1}{2}(\mathrm{LD}' \cdot \mathrm{LB} - \mathrm{LD} \cdot \mathrm{LB}') \\ & + (-\mathrm{LD}\,\cos 2\theta + \mathrm{LD}'\,\sin 2\theta)\sin\alpha \\ & + \left(P_x^2 - P_y^2\right)\sin 2\alpha\,\left(-\mathrm{LB}\,\cos 2\theta + \mathrm{LB}'\,\sin 2\theta\right) \end{aligned} \tag{3}$$

where $CD_{iso}$ is the isotropic CD which is independent of sample orientation; LD (LD') and LB (LB') are the linear dichroism (LD) and linear birefringence (LB) associated with the *x* and *y* (*x*' and y'; with a + 45° shift of the *x* and *y* axes) axes, respectively. $\theta$ is the angle of sample rotation around the optical axis, $\alpha$ is associated with the residual birefringence of the photoelastic modulator of the CD machine, and *a* is the azimuth angle of the photomultiplier with respect to the vertical axis. $P_x^2$ and $P_y^2$ are related to the transmittance of the detector in the *x* and *y* axes. The second term in the equation represents the interference of anisotropic LD and LB, giving rise to generation of artificial CD.[39,44] This interference leads to a sign inversion in the CD spectra when the incident light is flipped.[45] The third and fourth periodic terms correspond to the contributions of a residual linear polarization, which can introduce spurious CD by interacting with macroscopic anisotropies (LD or LB) of solid sample, depending on the rotation of sample.

*Transmissive Chiral EC Display Demonstration*: A transmissive chiral EC display devices were fabricated using patterned chiral EC layer on ITO, electrolyte solution, and ion storage layer deposited on ITO glass in the same way to unit device. Three different light sources (D65, TL84, and incandescent A) were supplied from MM-1e (GTI Graphic Technology). The transmissive chiral EC display was placed in the center of the chamber of MM-1e. The photographic images and supporting video were recorded at a distance of 30 cm from the sample. The linear polarizer and quarter-waveplate were equipped on the front of the digital camera in the same way as the dissymmetric transmission was measured in unit device using UV–vis–IR spectroscopy.

## Supporting Information

Supporting Information is available from the Wiley Online Library or from the author.

## Acknowledgements

The authors are grateful for the financial support from Ambilight Inc under work-for-hire contract #4000187.02. Special thanks to Azzaya Khasbaatar in Prof. Ying Diao's group at University of Illinois at Urbana Champaign (UIUC) for obtaining the GIXD data.

## Conflict of Interest

Jianguo Mei is the co-founder of Ambilight Inc, which sponsors this research

## Author Contributions

I.S. and J.M. conceived the project and planned the experiments. I.S. performed instrumental analyses and device characterization. L.Y. carried out synthesis of electrochromic polymers. K.C. assisted in electrochromic device fabrication. W-J. L. synthesized the ion storage materials and contributed to the instrumental analyses. I.S. and J.M. drafted the manuscript, and all authors contributed to writing the paper and feedback on the manuscript.

## Data Availability Statement

The data that support the findings of this study are available in the supplementary material of this article.

## Keywords

circularly polarized light, display, electrochromics, polarization, polymer

Received: July 17, 2023
Revised: October 17, 2023
Published online:

[1] J. F. Sherson, H. Krauter, R. K. Olsson, B. Julsgaard, K. Hammerer, I. Cirac, E. S. Polzik, *Nature* **2006**, *443*, 557.
[2] W. Zhang, T. Van Leent, K. Redeker, R. Garthoff, R. Schwonnek, F. Fertig, S. Eppelt, W. Rosenfeld, V. Scarani, C. C.-W. Lim, H. Weinfurter, *Nature* **2022**, *607*, 687.
[3] H.-S. Zhong, H. Wang, Y.-H. Deng, M.-C. Chen, L.-C. Peng, Y.-H. Luo, J. Qin, D. Wu, X. Ding, Y. Hu, P. Hu, X.-Y. Yang, W.-J. Zhang, H. Li, Y. Li, X. Jiang, L. Gan, G. Yang, L. You, Z. Wang, L. Li, N.-L. Liu, C.-Y. Lu, J.-W. Pan, *Science* **2020**, *370*, 1460.
[4] R. Naaman, Y. Paltiel, D. H. Waldeck, *Nat. Rev. Chem.* **2019**, *3*, 250.
[5] P. Lodahl, S. Mahmoodian, S. Stobbe, A. Rauschenbeutel, P. Schneeweiss, J. Volz, H. Pichler, P. Zoller, *Nature* **2017**, *541*, 473.
[6] C. Chappert, A. Fert, F. N. Van Dau, *Nat. Mater.* **2007**, *6*, 813.
[7] M. Schadt, *Annu. Rev. Mater. Sci.* **1997**, *27*, 305.
[8] G.-Y. Lee, J.-Y. Hong, S. Hwang, S. Moon, H. Kang, S. Jeon, H. Kim, J.-H. Jeong, B. Lee, *Nat. Commun.* **2018**, *9*, 4562.
[9] X. Guo, J. Zhong, B. Li, S. Qi, Y. Li, P. Li, D. Wen, S. Liu, B. Wei, J. Zhao, *Adv. Mater.* **2022**, *34*, 2103192.
[10] G. Yang, Y. Yu, B. Yang, T. Lu, Y. Cai, H. Yin, H. Zhang, N.-N. Zhang, L. Li, Y.-M. Zhang, S. X.-A. Zhang, *Angew. Chem., Int. Ed.* **2021**, *60*, 2018.
[11] X. Zhan, F.-F. Xu, Z. Zhou, Y. Yan, J. Yao, Y. S. Zhao, *Adv. Mater.* **2021**, *33*, 2104418.
[12] J. Yan, S.-T. Wu, K.-L. Cheng, J.-W. Shiu, *Appl. Phys. Lett.* **2013**, *102*, 081102.
[13] J. R. Brandt, X. Wang, Y. Yang, A. J. Campbell, M. J. Fuchter, *J. Am. Chem. Soc.* **2016**, *138*, 9743.
[14] J. Zhang, C. Meng, J. Huang, L. Jiang, D. Zhou, R. Chen, F. Yeung, H.-S. Kwok, P. Xu, G. Li, *Adv. Opt. Mater.* **2020**, *8*, 1901824.
[15] M. Li, S.-H. Li, D. Zhang, M. Cai, L. Duan, M.-K. Fung, C.-F. Chen, *Angew. Chem., Int. Ed.* **2018**, *57*, 2889.
[16] L. Xu, C. Wang, Y.-X. Li, X.-H. Xu, L. Zhou, N. Liu, Z.-Q. Wu, *Angew. Chem., Int. Ed.* **2020**, *59*, 16675.
[17] S. Feuillastre, M. Pauton, L. Gao, A. Desmarchelier, A. J. Riives, D. Prim, D. Tondelier, B. Geffroy, G. Muller, G. Clavier, G. Pieters, *J. Am. Chem. Soc.* **2016**, *138*, 3990.
[18] L. Wan, J. Wade, F. Salerno, O. Arteaga, B. Laidlaw, X. Wang, T. Penfold, M. J. Fuchter, A. J. Campbell, *ACS Nano* **2019**, *13*, 8099.
[19] L. Wan, X. Shi, J. Wade, A. J. Campbell, M. J. Fuchter, *Adv. Opt. Mater.* **2021**, *9*, 2100066.
[20] D.-M. Lee, J.-W. Song, Y.-J. Lee, C.-J. Yu, J.-H. Kim, *Adv. Mater.* **2017**, *29*, 1700907.
[21] D. Di Nuzzo, C. Kulkarni, B. Zhao, E. Smolinsky, F. Tassinari, S. C. J. Meskers, R. Naaman, E. W. Meijer, R. H. Friend, *ACS Nano* **2017**, *11*, 12713.
[22] L. Zhang, I. Song, J. Ahn, M. Han, M. Linares, M. Surin, H.-J. Zhang, J. H. Oh, J. Lin, *Nat. Commun.* **2021**, *12*, 142.
[23] T. Yasuda, K. Fujita, T. Tsutsui, Y. Geng, S. W. Culligan, S. H. Chen, *Chem. Mater.* **2005**, *17*, 264.
[24] B. A. San Jose, S. Matsushita, K. Akagi, *J. Am. Chem. Soc.* **2012**, *134*, 19795.
[25] K. Perera, W. Wu, L. You, J. F. Elman, Z. Wang, X. Wang, M. Ahmed, Z. Ke, J. Mei, *Macromolecules* **2023**, *56*, 480.
[26] Y.-Y. Lai, V.-H. Huang, H.-T. Lee, H.-R. Yang, *ACS Omega* **2018**, *3*, 18656.
[27] T. L. Myers, B. E. Bernacki, M. J. Wilhelm, K. L. Jensen, T. J. Johnson, O. M. Primera-Pedrozo, R. G. Tonkyn, S. C. Smith, S. D. Burton, A. M. Bradley, *Phys. Chem. Chem. Phys.* **2022**, *24*, 22206.
[28] L. De Marco, M. Thämer, M. Reppert, A. Tokmakoff, *J. Chem. Phys.* **2014**, *141*, 034502.
[29] I. Song, J. Ahn, H. Ahn, S. H. Lee, J. Mei, N. A. Kotov, J. H. Oh, *Nature* **2023**, *617*, 92.
[30] L. Wan, Y. Liu, M. J. Fuchter, B. Yan, *Nat. Photonics* **2023**, *17*, 193.
[31] N. Berova, L. D. Bari, G. Pescitelli, *Chem. Soc. Rev.* **2007**, *36*, 914.
[32] G. Albano, G. Pescitelli, L. Di Bari, *Chem. Rev.* **2020**, *120*, 10145.
[33] N. Harada, K. Nakanishi, N. Berova, in Comprehensive Chiroptical Spectroscopy, Volumte 2, **2012**, pp. 115–166.
[34] D. T. Christiansen, S. Ohtani, Y. Chujo, A. L. Tomlinson, J. R. Reynolds, *Chem. Mater.* **2019**, *31*, 6841.
[35] K. Perera, Z. Yi, L. You, Z. Ke, J. Mei, *Polym. Chem.* **2020**, *11*, 508.
[36] H. Goto, *J. Macromol. Sci. B* **2016**, *55*, 471.
[37] I. Zozoulenko, A. Singh, S. K. Singh, V. Gueskine, X. Crispin, M. Berggren, *ACS Appl. Polym. Mater.* **2019**, *1*, 83.
[38] R. Ghosh, F. C. Spano, *Acc. Chem. Res.* **2020**, *53*, 2201.
[39] A. Salij, R. H. Goldsmith, R. Tempelaar, *J. Am. Chem. Soc.* **2021**, *143*, 21519.
[40] X. Li, K. Perera, J. He, A. Gumyusenge, J. Mei, *J. Mater. Chem. C* **2019**, *7*, 12761.
[41] O. Arteaga, *Thin Solid Films* **2016**, *617*, 14.
[42] H. Han, Y. J. Lee, J. Kyhm, J. S. Jeong, J.-H. Han, M. K. Yang, K. M. Lee, Y. Choi, T.-H. Yoon, H. Ju, S.-K. Ahn, J. A. Lim, *Adv. Funct. Mater.* **2020**, *30*, 2006236.
[43] X. Li, Z. Wang, K. Chen, D. Y. Zemlyanov, L. You, J. Mei, *ACS Appl. Mater. Interfaces* **2021**, *13*, 5312.
[44] Y. Shindo, M. Nishio, S. Maeda, *Biopolymers* **1990**, *30*, 405.
[45] R. Kuroda, T. Harada, Y. Shindo, *Rev. Sci. Instrum.* **2001**, *72*, 3802.